Progress In Electromagnetics Research B, Vol. 66, 143–156, 2016

Analysis of Guided and Leaky TM_{0n} and TE_{0n} Modes in Circular Dielectric Waveguide

Siming Yang and Jiming Song*

Abstract—Guided and leaky modes for a circular dielectric rod are analyzed in detail in this paper. By considering the field distributions, these modes are well defined and classified. Through this research the relations for the mode solutions using different types of special functions and Riemann sheets are understood. Further, completed forms of characteristic equations used to solve different modes are presented explicitly. Asymptotic expansion method and Lambert W function are employed to derive the initial guesses around cutoff frequency, low frequency limit and high frequency limit for both TM and TE cases. The behaviors of complex transverse attenuation constants for proper and two types of improper modes with different cases are presented with some modes not shown in other works.

1. INTRODUCTION

Geometrical configurations based on circular rod are very popular, such as coaxial lines and cavities; these cylindrical structures maintain a uniform cross section along their length. However, due to conductor loss, the metallic based structures are impractical in high frequency region. A better option is to use a low-loss dielectric waveguide [1–3]. One of the well-known examples of this is optical fiber. In 1966, Kao [4] published a paper on the theory and practice of optical fiber for communication applications, which heralded the beginning of a new era in telecommunications. Investigation related to the guide modes has been well established even earlier than 1966 [5, 6], whereas the leaky modes below cutoff frequency have been scarcely investigated. Yet, the leaky wave is useful in many antenna applications [7–10]. Until 1969, Arnbak [11] found the complex propagation constant below the cutoff frequency by solving the asymptotic forms of the characteristic equation, thus, proving the existence of leaky modes in the circular dielectric waveguide. Later on, Sammut and Snyder [12] presented the characteristic of the leaky modes graphically for both lossless and lossy cases. However, these results were obtained based on approximation method, which led to the results not accurate enough for further applications.

Several decades later, Kim et al. studied the guided and leaky modes supported by the dielectric circular rod [13, 14], and demonstrated several lower orders of the modes by using the Davidenko's complex root finding algorithm. In addition, Kim et al. also defined and explained the regimes of these modes based on their physical meanings [15–18]. To solve the eigenvalue problems more efficiently, asymptotic formulas have been derived before using the numerical solvers for planar and circular multilayered structures [19–23]. The waveguides open to air or closed with perfect matching layer (PML) were considered, and Lambert W function [24, 25] has been leveraged frequently to simplify the asymptotic expressions. Solutions to dispersion equations with complex dielectric permittivity are considered [26] for microwave transfer in tubular sliding-mode plasma waveguides.

Received 8 December 2015, Accepted 10 March 2016, Scheduled 18 March 2016
* Corresponding author: Jiming Song (jisong@iastate.edu).
The authors are with the Department of Electrical and Computer Engineering, Iowa State University, Ames, IA 50011, USA.

However, through investigating these articles and relevant textbooks [27, 28], we find that there are still many ambiguous parts left unsolved. First of all, different special functions involved characteristic equations have been employed in different articles [11, 13] or textbooks [27, 28] to solve these modes problems. A same solution is achieved using different special functions for proper (guided) modes. Nevertheless, due to t multiple-value issue in the special functions, confusion and difficulty emerge for improper (leaky) modes. Secondly, it is also found that types of improper modes have not been demonstrated completely for both TM and TE cases in the previous works. The ways of obtaining and indexing these modes are unclear as well [13, 14].

Based on these considerations, this paper analyzes proper and improper modes by starting from the perspective of special functions to find the solutions supported by the circular dielectric waveguide. Accordingly, three kinds of special functions, Hankel function of the first kind ($H_m^{(1)}(\cdot)$), Hankel function of the second kind ($H_m^{(2)}(\cdot)$), and modified Bessel function ($K_m(\cdot)$), are analyzed in detail to find the relationship of the solutions when any one of the special functions is involved. Then, a set of completed forms of characteristic equations for different cases are explicitly exhibited.

Further, asymptotic expansion method [29] is employed to find the initial guess expressions for proper and improper modes based on the characteristic equations of TM and TE cases. The initial guess derivation of the hybrid (EH or HE) modes will not be discussed here, since the analysis will made this paper to an unacceptable length. It is believed that the idea of deriving the initial guess for both TM and TE cases can be further extended to derive the initial guess for the hybrid modes. In this process, analysis for the modes problem of dielectric slab [30–34] has been referred.

For completeness, initial guess expressions are derived from high and low frequency limits, and around cutoff frequency respectively. In this process, we leverage Lambert W function in some expressions. These completed initial guess expressions provide simple and efficient way of indexing these modes. Finally, Newton method is employed to determine the complex propagation constant of both proper and improper modes for TM and TE cases. The numerical results are verified by comparing with Kim's results [13].

2. FORMULATIONS AND EQUATIONS

2.1. Characteristic Equation

Assuming the time factor with convention e^{jwt}, by applying the continuity conditions of tangential fields to an infinite long homogenous circular dielectric waveguide with radius a embedded in an infinitely homogenous medium, the characteristic equation for TM and TE cases can be derived by imposing $m = 0$ from [27, 28], which means that the modes are without variations along the circular angle. Under this circumstance, the characteristic equation can be expressed as

$$\frac{\kappa}{u}\frac{J_1(u)}{J_0(u)} + \frac{1}{jv}\frac{H_1^{(2)}(-jv)}{H_0^{(2)}(-jv)} = 0 \tag{1}$$

By assigning $\kappa = \epsilon_{r1}/\epsilon_{r2}$ or $\kappa = \mu_{r1}/\mu_{r2}$, Eq. (1) represents TM or TE case, where ϵ_{ri} and μ_{ri} are the dielectric and magnetic constants, respectively. The second subscript $i = 1$ represents the region within the rod, and $i = 2$ represents the region outside the rod. For non-magnetic dielectric rod $\mu_{r1} = \mu_{r2} = 1$, thus $\kappa = 1$. $J_m(\cdot)$ and $H_m^{(2)}(\cdot)$ are the m-th order Bessel function of the first kind and Hankel function of the second kind. In Eq. (1), u and v are expressed as

$$u \triangleq k_0 a\sqrt{\mu_{r1}\epsilon_{r1} - \delta^2} \tag{2a}$$

$$v \triangleq k_0 a\sqrt{\delta^2 - \mu_{r2}\epsilon_{r2}} \tag{2b}$$

where k_0 is the wave number in free space. $\delta = k_z/k_0$, and k_z is the axial complex propagation constant. Therefore, r is given by

$$r = \sqrt{u^2 + v^2} = k_0 a\sqrt{\mu_{r1}\epsilon_{r1} - \mu_{r2}\epsilon_{r2}} \tag{3}$$

For Eq. (1), either u, v, or δ can be treated as an unknown. It is well known that the Hankel function of the second kind has a multiple-value property in a complex plane, and it is found that Eq.

(1) is an even function of u and δ. These properties of Eq. (1) make v as a variable directly a better choice. In this situation, the square root issue introduced by solving δ or u is directly avoided. Once v is solved, u and δ are expressed in terms of v explicitly. Eq. (2b) indicates that v describes the wave behavior along the radial direction outside the circular dielectric rod. By substituting v into the leading transverse wave form of the Hankel function, we have $e^{v\rho/a} = e^{-\mathrm{Re}(v)\rho/a}e^{-j\mathrm{Im}(v)\rho/a}$. It is clear that v is normalized complex transverse attenuation constant with the imaginary part for propagation constant. Accordingly, Table 1 presents the classification of different types of modes based on v, and these definitions will be used in the following discussion.

Table 1. Classification of different kinds of modes.

	Proper Modes	Improper Modes	
		Outging	Incoming
Sign(Re(v))	(+)	(−)	
Sign(Im(v))	(+,−)	(+)	(−)

2.2. Relationship between Propagation Constants with Special Functions

Besides expressing Eq. (1) in terms of $H_m^{(2)}(\cdot)$, the characteristic equation can also be expressed in terms of $K_m(\cdot)$, and $H_m^{(1)}(\cdot)$ with different arguments

$$\frac{\kappa}{u}\frac{J_1(u)}{J_0(u)} + \frac{1}{v}\frac{K_1(v)}{K_0(v)} = 0 \tag{4}$$

$$\frac{\kappa}{u}\frac{J_1(u)}{J_0(u)} - \frac{1}{jv}\frac{H_1^{(1)}(jv)}{H_0^{(1)}(jv)} = 0 \tag{5}$$

With these relationships between different special functions [35], we can qualitatively conclude the relationship between the solutions of Eqs. (4), (5), and (1): for the proper modes, v is in the first and fourth quadrants. As all three equations with different special functions give the same solutions

$$v_{np}^{K} = v_{np}^{H_1} = v_{np}^{H_2} \tag{6}$$

The superscripts H_2, K, and H_1 mean the solution from Eqs. (1), (4), and(5), respectively. The subscript stands for the n-th modes in the p-th Riemann sheet. For the outgoing improper mode, v is in the second quadrant.

$$v_{np}^{K} = v_{n(p+1)}^{H_1} = v_{np}^{H_2} \tag{7}$$

Similarly, for the incoming improper mode, we have

$$v_{n(p+1)}^{K} = v_{n(p+1)}^{H_1} = v_{np}^{H_2} \tag{8}$$

2.3. Complex Conjugate Properties for Lossless Rod

To make this study more complete, the properties related to the relationship of solution and their corresponding complex conjugate are presented. These conclusions, on one hand, give a better understanding of this work, and on the other hand, they help us avoid some unnecessary trouble through the numerical implementation.

From the complex conjugate relationship of special functions in their principal values [24], we have the general complex conjugate relationships for special functions in different Riemann sheets as

$$K_{mp}(z^*) = K_{m(-p)}^*(z) \tag{9}$$

$$H_{mp}^{(1)}(z^*) = H_{m(-p)}^{(2)*}(z) \tag{10}$$

$$H_{mp}^{(2)}(z^*) = H_{m(-p)}^{(1)*}(z) \tag{11}$$

Equations (9)–(11) indicate that, for the principal value, namely $p = 0$, $[v_n^K]^*$, $[v_n^{H_1}]^*$, and $[v_n^{H_2}]^*$ are the solutions as well for the lossless dielectric rod. For the p-th Riemann sheet, we have $[v_n^K]^* = v_{n(-p)}^K$, $[v_n^{H_1}]^* = v_{n(-p)}^{H_2}$, and $[v_n^{H_2}]^* = v_{n(-p)}^{H_1}$, respectively. From the above analysis, the relationship of the complex conjugate solutions corresponding to different types of modes can be concluded as

$$[v_{np}^K]^* = [v_{np}^{H_1}]^* = [v_{np}^{H_2}]^* = v_{n(-p)}^K = v_{n(-p)}^{H_2} = v_{n(-p)}^{H_1} \tag{12}$$

for the proper modes in the first and fourth quadrants, and

$$[v_{np}^K]^* = [v_{n(p+1)}^{H_1}]^* = [v_{np}^{H_2}]^* = v_{n(-p)}^K = v_{n(-p-1)}^{H_2} = v_{n(-p)}^{H_1} \tag{13}$$

for the improper modes in the second quadrant, and

$$[v_{n(p+1)}^K]^* = [v_{n(p+1)}^{H_1}]^* = [v_{np}^{H_2}]^* = v_{n(-p-1)}^K = v_{n(-p-1)}^{H_2} = v_{n(-p)}^{H_1} \tag{14}$$

for the improper modes in the second quadrant. Due to the relationship in the modes solved using different special functions, the following sections will focus on the results solved based on $H_m^{(2)}(\cdot)$ as shown in Equation (1).

3. INITIAL GUESSES

Among several iterative methods, due to the advantages of easy implementation, converging fast, and requiring only one initial guess, Newton-Raphson method is employed to solve Equation (1) numerically. Appropriate initial guess is crucial in finding right solutions with smaller number of iterations. In this section, the initial guesses are derived using the asymptotic form on the $p = 0$ Riemann sheet. By considering the behavior of u and v in different regions, Eq. (1) is expanded around cutoff frequency, high frequency limit as well as the low frequency limit. From numerical solutions, it is found that from none of the perspectives mentioned above we can solve three types of modes completely, due to the different types of modes distributed in different regions. The incoming improper modes are further categorized as ones stopping at the cutoff frequency and ones stopping at DC. In this asymptotic expansion process, we will introduce the Lambert W function [24, 25] with different branches to find accurate and simple forms of initial guesses for both TM and TE cases.

3.1. Around the Cutoff Frequency

In the circular dielectric rod, TM_{0n} and TE_{0n} modes share the same cut-off frequency. This can be derived by imposing $v = 0$, which leads to $J_0(u = \chi_{0n}) = 0$, where χ_{0n} denotes the n-th root of zero order Bessel function of the first kind. Thus, around the cut-off frequency we have $r \approx \chi_{0n}$, $0 \approx v \ll r$, and $u \approx r - v^2/(2r)$. By expanding the Hankel function of the second kind with small argument, the inverse of the second term in Equation (1) is approximated as

$$-jv\frac{H_0^{(2)}(-jv)}{H_1^{(2)}(-jv)} \approx v^2 \ln(ve^{\gamma}/2) \tag{15}$$

where $\gamma \approx 0.577215664$ is the Euler-Mascheroni constant. Similarly, we can expand Bessel function of the first kind around r and get the inverse of the first term as

$$\frac{u}{\kappa}\frac{J_0(u)}{J_1(u)} = c_1(r) + \frac{v^2}{4\kappa} \tag{16}$$

with $c_1(r) = -\chi_{0n}(r - \chi_{0n})$. By combining Eqs. (15) and (16), Eq. (1) is simplified as

$$v^2 \ln(v^2 a_1^2/4) = 2c_1(r) \tag{17}$$

with $a_1 = e^{\gamma - 1/2\kappa}$. The solution corresponding to Eq. (17) is represented by Lambert W function [24, 25] as

$$v = 2a_1^{-1} e^{\frac{1}{2}W_p(z(r))} \tag{18}$$

where subscript p represents different branches of $W(z)$ and $z(r) = a_1^2 c_1/2$. Sommerfeld derived a form similar to Eq. (17) for waves over lossy wires [37] (p.183) using asymptotic representation of Bessel functions, but Eq. (17) keeps more terms as shown in Eq. (16) by expanding the Bessel functions around the cut-off. Sommefeld's solution is in a form corrected step by step in the subsequent approximations [37] (p.183), not the closed form solutions as shown in Eq. (18) using Lambert W functions. The initial guess expression in Eq. (18) can predict different types of modes with appropriate branches of Lambert W function, which are summarized as in Table 2.

Table 2. Corresponding branches to derive different types of modes.

	Proper Modes	Improper Modes	
		Outging	Incoming
p value	-1	1	
Sign$(r - \chi_{0n})$	$(+)$	$(-)$	$(+)$
Sign(z)	$(-)$	$(+)$	$(-)$

The initial guesses given by Eq. (18) around cutoff frequency are very close to the true solutions for different types of modes, which are illustrated in Fig. 1. These initial guesses are derived based on the leading term expansion of Eq. (1), which takes into account both efficiency and accuracy [36].

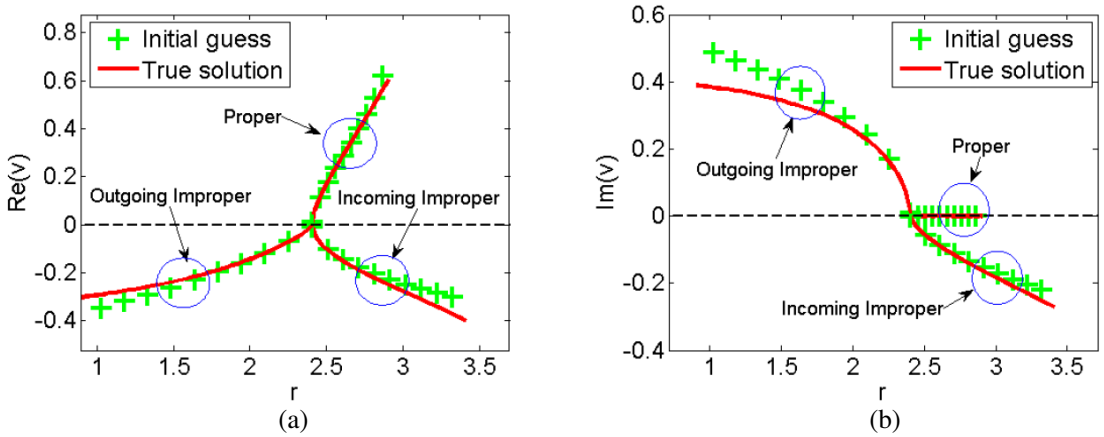

Figure 1. With $\kappa = 4$, the initial guesses are compared with the accurate numerical solutions around the first cutoff frequency.

3.2. High Frequency Limit

3.2.1. Case with $|v| \gg |u| \gg 1$

In the high frequency region ($r \gg 1$), both u and v are large, namely $v \gg 1$ and $u \gg 1$. Also, in this region $\delta = k_z/k_0$ approaches $\sqrt{\epsilon_{r1}\mu_{r1}}$, which makes $v \gg u$. Under this circumstance, $J_m(\cdot)$ and $H_m^{(2)}(\cdot)$ are expanded with large argument [24, 29] by considering the argument in different regions. When the phase of argument is away from the negative real axis, Eq. (1) is approximated as

$$\tan(u - \pi/4) = -u/(\kappa v) \tag{19}$$

For proper modes, the primary form of v_0 can be derived from Eq. (2b) as $v_0 = \sqrt{r^2 - u_0^2}$. By substituting this v_0 expression into Eq. (19), a set of more accurate initial guess expressions for proper

modes are obtained as

$$u_1 = \frac{\pi}{4} + m\pi - \tan^{-1}\left(\frac{1}{\kappa}\frac{u_0}{\sqrt{r^2-u_0^2}}\right) \tag{20a}$$

$$v_1 = \sqrt{r^2-u_1^2}, \quad m = 0, 1, 2, ... \tag{20b}$$

For the improper modes in the third quadrant, the primary form of v_0 is written as $v_0 = -\sqrt{r^2-u_0^2}$. Following the same steps, more accurate initial guess expressions for incoming improper modes are written as

$$u_1 = \frac{\pi}{4} + m\pi + \tan^{-1}\left(\frac{1}{\kappa}\frac{u_0}{\sqrt{r^2-u_0^2}}\right) \tag{21a}$$

$$v_1 = -\sqrt{r^2-u_1^2}, \quad m = 0, 1, 2, ... \tag{21b}$$

3.2.2. Case with $|u| \gg |v| \gg 1$

Equation (21) can be used to predict incoming improper modes for TM and TE cases for the high frequency limit. Another type of solution at the high frequency is $|u| \gg |v| \gg 1$. From this we observe that the argument $z = -jv$ is in the second quadrant and close to the negative real axis. Using the expansion of $H_m^{(2)}(\cdot)$ given in Eq. (A7), we have

$$\tanh(v + j\pi/4) = -\frac{1-3a(v)}{3-a(v)} \tag{22}$$

where $a(v) = \kappa\frac{v}{u}\frac{J_1(u)}{J_0(u)}$, thus the initial guess for the incoming improper modes is expressed as

$$v_0 = -\tanh^{-1}(1/3) + j(m-1/4)\pi, \quad m = -1, -2, -3, ... \tag{23a}$$

$$v_1 = -\tanh^{-1}\left(\frac{1-3a(v_0)}{3-a(v_0)}\right) + j(m-1/4)\pi \tag{23b}$$

3.3. Low Frequency Limit

3.3.1. $\kappa \neq 1$ (TM Case)

At low frequency range ($r = 1$), due to the solution for two types of improper modes located in different regions, the corresponding special functions are expanded in different ways. At DC limit, right hand side of Eq. (3) approaches zero, namely $u^2+v^2 = 0$, and we have $u \approx -jv$ and $v \approx ju$. For the improper modes in the second quadrant, v is in the second quadrant and close to the positive imaginary axis, thus $u \approx -jv$ is in the first quadrant and close to the positive real axis. This indicates that Eq. (19) can still be employed to derive the initial guess for the outgoing improper modes. According to the previous discussion, the primary forms of initial guess for the outgoing improper modes are expressed as

$$u_0 = \pi/4 + m\pi + j\tanh^{-1}(1/\kappa), \quad m = 0, 1, 2, ... \tag{24a}$$

$$v_0 = -\sqrt{r^2-u_0^2} \approx j(\pi/4 + m\pi) - \tanh^{-1}(1/\kappa) \tag{24b}$$

However, for the incoming improper modes stopping at DC limit, variable v is around the negative imaginary axis; therefore, $u \approx -jv$ is in the second quadrant and close to the negative real axis. In this situation, both $H_m^{(2)}(-jv)$ and $J_m(u)$ have to be expanded around negative real axis, which are shown in Eqs. (A3) and (A7). Correspondingly, Eq. (1) is in a new asymptotic form

$$\tan(u + \pi/4) = \frac{ju}{v}\frac{1}{\kappa}\frac{3\tan(u+\pi/4) - j}{3 + j\tan(u+\pi/4)} \tag{25}$$

For $\kappa \neq 1$, it can be further reduced as

$$\tan(u+\pi/4) = \frac{1}{\kappa}\frac{3\tan(u+\pi/4)-j}{3+j\tan(u+\pi/4)} \tag{26}$$

In this quadratic equation $\tan(u+\pi/4)$ is treated as a variable. After neglecting one solution which contradicts the assumption, we have

$$\tan(u+\pi/4) = j\tilde{\kappa} \tag{27}$$

where $\tilde{\kappa} = \left[3(\kappa-1)+\sqrt{9(\kappa-1)^2+4\kappa}\right]/(2\kappa)$. Therefore, the initial guess for the incoming improper modes stopping at DC limit is expressed as

$$u_0 = \pi/4 + m\pi + j\tanh^{-1}(1/\tilde{\kappa}), \quad m = -1,-2,-3,... \tag{28a}$$

$$v_0 = -\sqrt{r^2-u_0^2} \approx j(\pi/4+m\pi) - \tanh^{-1}(1/\tilde{\kappa}) \tag{28b}$$

3.3.2. $\kappa = 1$ (TE Case)

Equations (24) and (28) are only applicable for $\kappa \neq 1$, as TM case. To generate the expressions for TE case with $\kappa = 1$, we first examine the value of u at DC limit and find that u has a large value for the imaginary part. As a matter of fact, we assume that u is in the form of

$$u = \pi/4 + m\pi + ju_I, \quad m = 0,1,2,\ldots \tag{29}$$

where subscript I represents the imaginary part of u. By substituting it into Eq. (19), according to Eqs. (B1)–(B3), we have

$$u_I = W_{-1}(-r/2) \tag{30}$$

Similarly, for the incoming improper modes stopping at DC limit, we still assume that u in Eq. (25) has the same form of Eq. (29) but with $m = -1,-2,-3,\ldots$. Following the same procedure, as shown in Eq. (B4), u_I is approximated as shown in Eq. (30) as well. Consequently, the initial guess of outgoing improper modes and incoming improper modes stopping at DC limit for TE case are expressed as

$$u_0 = \pi/4 + m\pi + jW_{-1}(-r/2) \tag{31a}$$

$$v_0 = -\sqrt{r^2-u_0^2} \approx j(\pi/4+m\pi) - W_{-1}(-r/2) \tag{31b}$$

A similar expression is derived for k_z for high-order leaky modes in [21, 22] using Lambert W function.

4. NUMERICAL RESULTS AND DISCUSSIONS

The guided and leaky modes of circular waveguide are solved numerically using the initial guesses derived from last section around the cut-off frequency and the high or low frequency limits. The solutions using the second kind of Hankel function on the principal plane are presented in this section. Using the relationship from last section, the solutions using other special functions or in different Riemann sheets can be found. For most examples, normalized complex transverse attenuation constant v is shown because it defines different mode properties as listed in Table 1.

Several low-order proper and outgoing improper modes are shown in Fig. 2. For the proper modes, there is no propagation in the transverse direction, and it has positive attenuation constant above the cutoff frequency, which is exhibited in Fig. 2(a). For the convenience of visualization, the attenuation constant v for the proper modes are normalized with $k_0 a$. These curves are generated either from the cutoff frequency using initial guesses according to Section 3.1 or from the high frequency limit in Eq. (20). Also from the analysis in the high frequency limit, the asymptotic value for the upper bound is $\sqrt{\mu_{r1}\epsilon_{r1}-\mu_{r2}\epsilon_{r2}}$. As the operating frequency decreases to the cutoff frequency, the proper modes will vanish and finally convert into the outgoing improper modes. This set of outgoing improper modes can be generated by using the initial guesses derived in Section 3.1 or using the initial guesses from the

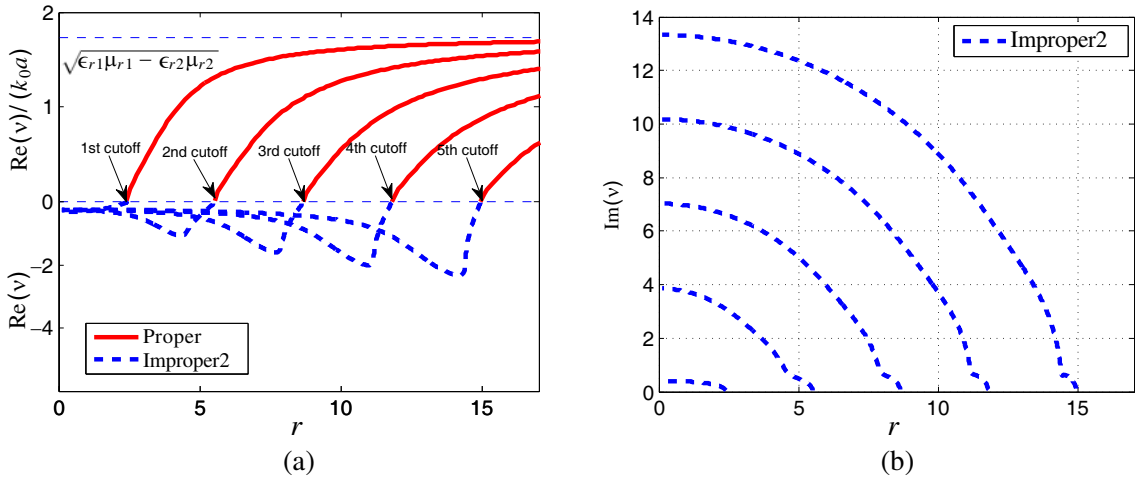

Figure 2. Complex transverse attenuation constants for several low orders proper and outgoing improper modes with $\kappa = 4$. (a) Real parts. (b) Imaginary parts. The Improper2 in the legend represents the outgoing improper modes in the second quadrant.

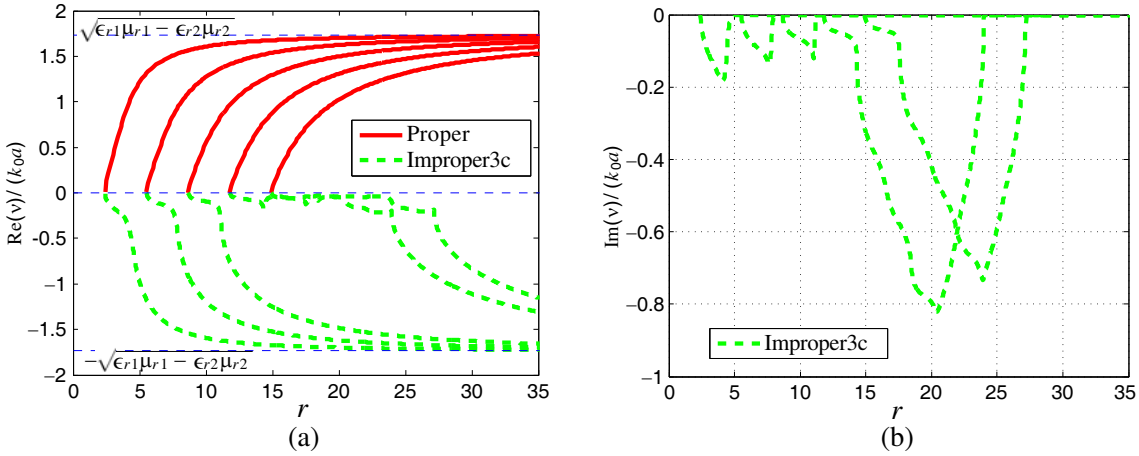

Figure 3. Complex transverse attenuation constants for the low order incoming improper mode stop at cutoff frequency with $\kappa = 4$. (a) Real parts. (b) Imaginary parts. The Improper3c in the legend represents the incoming improper in the third quadrant stops at the cutoff frequency.

low frequency limit with Eq. (24). Further, they are well indexed from low to high order, according to integer m in Eq. (24). Some discussions of the physical meaning on the outgoing improper modes have been presented by Kim et al. in [14] and will not be duplicated here.

Compared to the outgoing improper modes, the incoming improper modes presented in Fig. 3 have the opposite sign for the attenuation constants. The magnitude for these two types of improper modes increases in the direction away from the waveguide but propagating in the opposite directions transversely. This set of incoming improper modes which stop at cutoff frequency can be predicted by using the initial guess expressions in Eq. (18) with $p = 1$ around the each cutoff frequency or by using the initial guess expressions in Eq. (21) at high frequency limit. From the high frequency limit, the asymptotic lower bound is $-\sqrt{\mu_{r1}\epsilon_{r1} - \mu_{r2}\epsilon_{r2}}$.

However, for $\kappa = 4$, except the first three low-order modes, the index in Eq. (24) is not in a one-to-one relationship with the order of modes stopping at cutoff frequency. For instance, the incoming improper mode stopping at the fourth cutoff frequency is indexed with $m = 7$ from Eq. (21). The reason is that Eq. (21) generates not only a set of incoming improper modes ending up at the cutoff

frequency, but also another type of incoming modes stopping at DC, which have not been presented before. For this type of incoming improper modes stopping at DC, they can be predicted from the DC limit by using Eq. (28) or Eq. (21).

It is observed from Fig. 4 that the imaginary part of v is much larger than the real part for the incoming improper modes at DC. This is similar for the outgoing improper modes shown in Fig. 2, which implies that the imaginary part is dominant in deriving the initial guess at DC limit for both the incoming improper modes and the outgoing improper modes. The corresponding values are $\mathrm{Im}(v) = \pi/4 + m\pi$ for the outgoing case with $m = 0, 1, 2\ldots$ and $m = -1, -2, -3\ldots$ for the incoming case. As the absolute value of index m increases, the initial guess will be more accurate than the true value. In contrast, the real part of v is close to a relative small constant at DC limit for both the outgoing and incoming cases. According to Eqs. (24b) and (28b), with $\kappa = 4$, the real parts are very close to $-\tan^{-1}(1/\kappa) \approx -0.2554$ and $-\tanh^{-1}(1/\tilde{\kappa}) \approx -0.4531$ respectively. These values are well matched with the numerical results shown in Fig. 2(a) and Fig. 4(a) at DC limit.

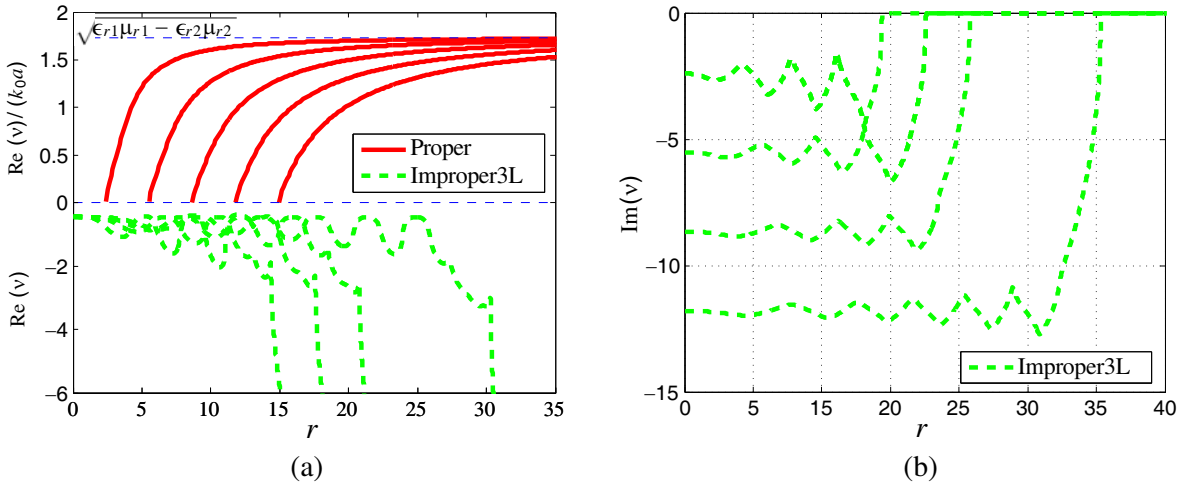

Figure 4. Complex transverse attenuation constants for the low order incoming improper mode stop at DC with $\kappa = 4$. (a) Real parts. (b) Imaginary parts. The Improper3L in the legend represents the incoming improper in the third quadrant stops at the low frequency limit.

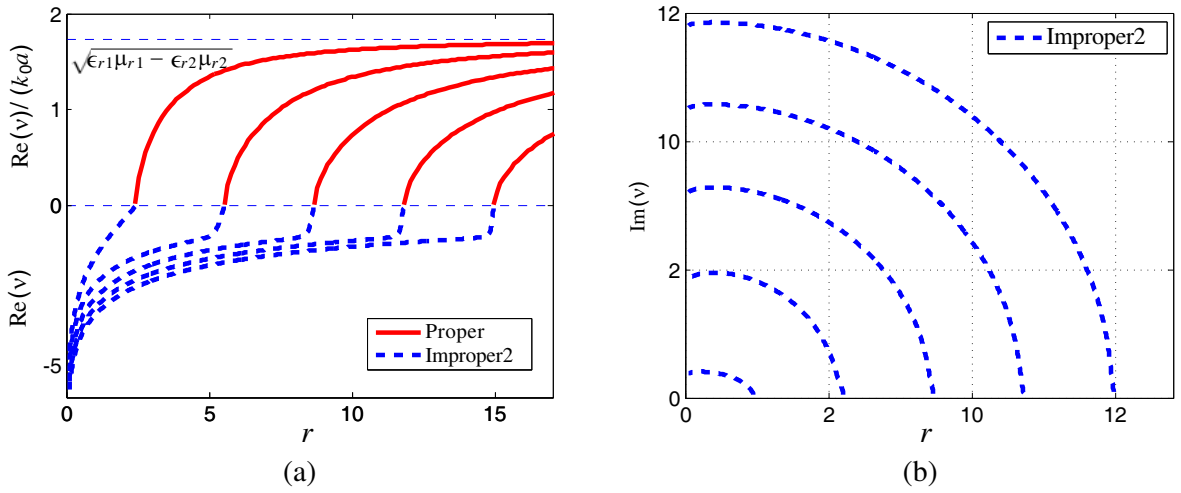

Figure 5. Transverse attenuation constants for several low orders proper modes and outgoing improper modes with $\kappa = 1$. (a) Real parts. (b) Imaginary parts.

The proper modes exhibited here are physical modes, which form a complete set and can generally describe an arbitrary field [38]. Correspondingly, the incoming improper modes are nonphysical modes [38], and the wave propagates and decays in region 1 and has an exponential growth in the transverse direction in region 2 [39].

The way of deriving the complex transverse propagation constants for TE case is very similar to TM case by using the initial guesses derived in Section 3, except for the set of initial guess expressions at DC limit for two types of improper modes and the initial guess at high frequency limit for the incoming improper modes. The transverse attenuation constants of several low-order proper modes and outgoing improper modes for $\kappa = 1$ are shown in Fig. 5. From Fig. 2(a), it is found that the proper modes are always well behaved from cutoff frequency to the high frequency limit. However, for the outgoing improper modes, the real part of v will stop at DC limit with different values. Due to the different values of κ, the real parts of v are close to $-W_{-1}(-r/2)$ for $\kappa = 1$, and $\tanh^{-1}(1/\kappa)$ for $\kappa \neq 1$ at DC limit. The behavior of the imaginary parts for $\kappa = 1$ case is very close to $\kappa \neq 1$ case, and it is not shown here to save space.

Figure 6(a) plots the transverse attenuation constant for the low-order incoming improper mode

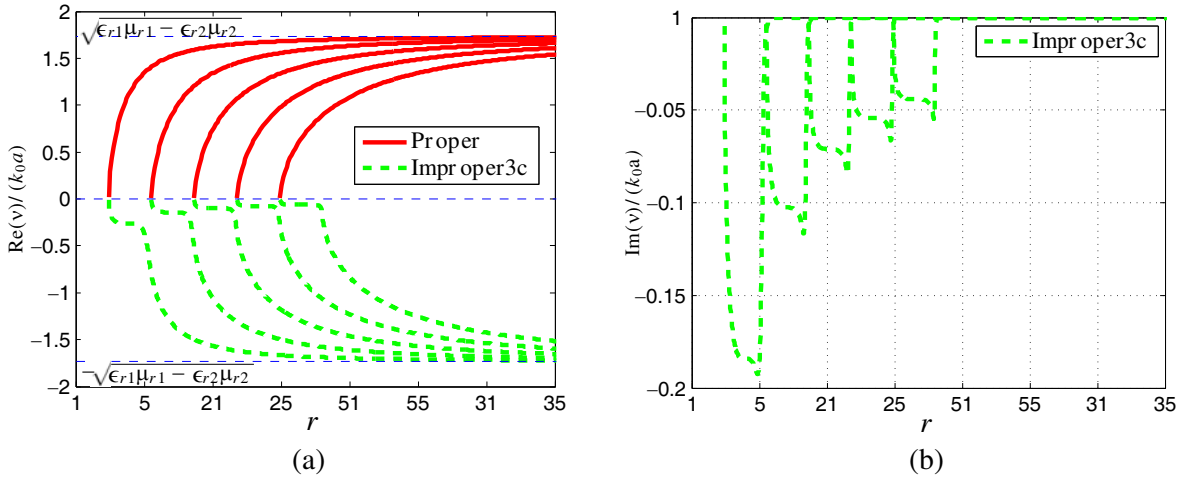

Figure 6. Complex transverse attenuation constants for the low order incoming improper mode stop at cutoff frequency with $\kappa = 1$. (a) Real part. (b) Imaginary part.

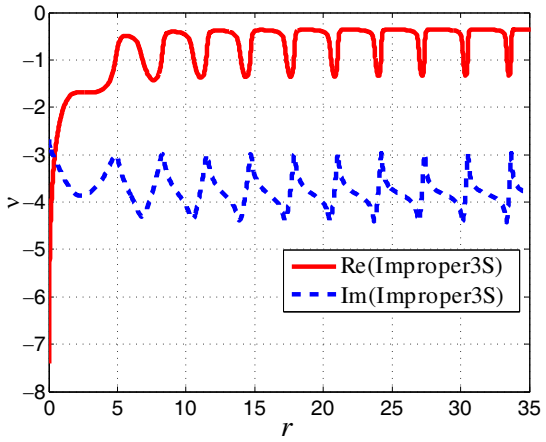

Figure 7. Both the real and imaginary part of the complex transverse attenuation constant for the first TE incoming improper mode ($m = 1$) with $\kappa = 1$. The Improper3S in the legend represents the special case of incoming improper modes in the third quadrant.

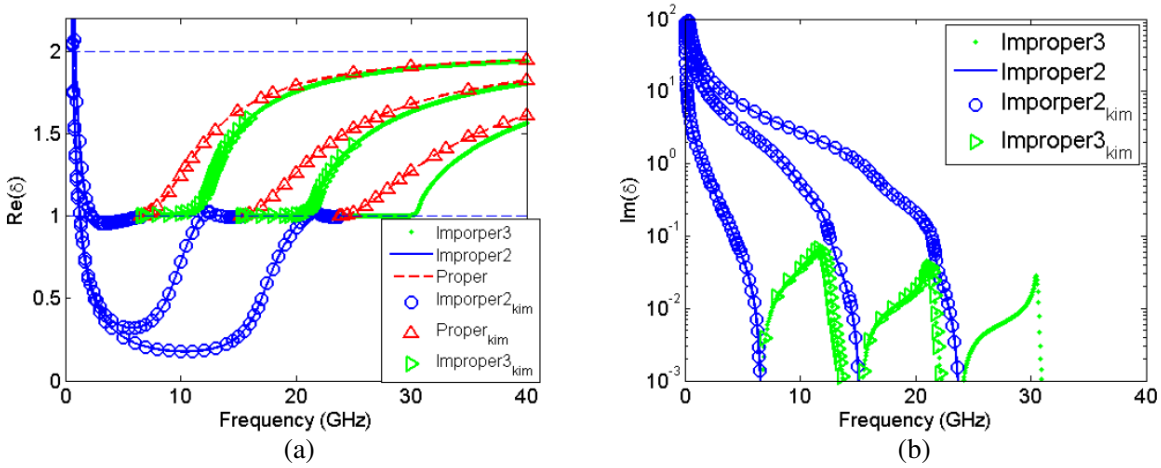

Figure 8. The complex longitudinal propagation constants for low order proper, and two types of improper modes. (a) Real part. (b) Imaginary part. The radius for the rod is $a = 0.01$ m, and the dielectric constants inside and outside the rod are $\epsilon_{r1} = 4$ and $\epsilon_{r2} = 1$ respectively.

stopping at the cutoff frequency. Similarly, by comparing with Fig. 3, it is found that the dispersion curves are smoother for the higher modes with $\kappa = 1$. However, for the incoming improper modes ending up at the DC, the behavior for the TE case shown in Fig. 7 is different from the TM case. Besides the different values at DC limit, v will approach a constant value through the whole range for both the real and imaginary parts.

Our verifications are made by comparing our results with Kim's results [13]. The expression of the normalized longitudinal propagation constant $\delta = k_z/k_0$ can be derived from Eq. (2b) with given v. Both the real and imaginary parts for several low-order modes are illustrated in Fig. 8. An agreement has been reached between our results and Kim's results. For the other high-order incoming improper modes, they are examined by substituting the numerical results into Eq. (1), and the relative error is down to 10^{-10}.

5. CONCLUSIONS

In this paper, three kinds of special functions are used to solve the characteristic equation for the modes supported by circular dielectric waveguide. The corresponding solutions are well defined and classified with the field distribution. Based on different special functions and Riemann sheets, their relationships are concluded through Eqs. (6)–(8). The complete forms of characteristic equations to solve proper and two types of improper modes are presented explicitly. In addition, the properties of the complex conjugate of the corresponding solutions for lossless dielectric rod are presented to make this study more complete.

The relative accurate initial guesses are derived to accelerate the convergence in finding the modes. The asymptotic expansions for both Bessel and Hankel functions are derived for large argument near the negative real axis. Around cutoff frequency, Lambert W functions at different branches are employed to find the initial guesses for the proper modes, outgoing improper modes, and incoming improper modes stopping at cutoff frequency. At the low frequency limit, we predict the whole set of outgoing improper modes and incoming improper modes stopping at DC. Also, the initial guesses for the whole set of proper and incoming improper modes from the high frequency limit are also derived. Further, we have made the initial guesses applicable to both TM and TE cases by carefully testing different values of κ. Finally, complex transverse attenuation constants for both TM and TE cases are presented with some modes not shown in other works.

APPENDIX A. THE ASYMPTOTIC APPROXIMATIONS FOR BESSEL AND HANKEL FUNCTIONS IN DIFFERENT REGIONS

Bessel function of the first kind and Hankel function of the second kind expanded as [24]

$$J_m(z) \sim \sqrt{\frac{2}{\pi z}} \cos(z - \frac{m\pi}{2} - \frac{\pi}{4}) \tag{A1}$$

and

$$H_m^{(2)}(z) \sim \sqrt{\frac{2}{\pi z}} e^{-j(z - \frac{m\pi}{2} - \frac{\pi}{4})} \tag{A2}$$

when $|\arg z| < \pi$. By considering $m = 0$ and $m = 1$, we have $J_1(z)/J_0(z) \approx \tan(z - \pi/4)$ and $H_1^{(2)}(z)/H_0^{(2)}(z) \approx j$. After substituting these two expressions into Eq. (1), Eq. (19) is achieved. From Section 3.2 we know that at high frequency range $|v| \gg |u| \gg 1$. When $|\arg z| < \pi$, $J_m(\cdot)$ is expanded as

$$J_m(z) \sim (-1)^m \sqrt{\frac{-2}{\pi z}} \cos(z + \frac{m\pi}{2} + \frac{\pi}{4}) \tag{A3}$$

by using $J_m(z) = (-1)^m J_m(-z)$.

Now, let us derive the asymptotic approximation of the Hankel function for argument z in the second quadrant above the negative real axis and close to π. We know that $H_m^{(2)}(z) = J_m(z) - jY_m(z)$, where $Y_m(z)$ is the Bessel function of the second kind. The phase angle of z is close to π, thus $J_m(-z)$ and $H_m^{(2)}(-z)$ can be well approximated according to Eqs. (A1)–(A2). To express $H_m^{(2)}(z)$ in terms of $J_m(-z)$ and $H_m^{(2)}(-z)$, we can use

$$Y_m(ze^{jn\pi}) = e^{-jnm\pi} Y_m(z) + 2j \sin(nm\pi) \cot(m\pi) J_m(z) \tag{A4}$$

where m is the order of special function, and n is an integer. For $n = -1$, $ze^{-j\pi} = -z$ is in the fourth quadrant near the positive real axis, and the rotation from z to -z does not cross the branch cut.

$$Y_m(z) = (-1)^m \left[Y_m(-z) + 2jJ_m(-z)\right] \tag{A5}$$

By substituting $J_m(z) = (-1)^m J_m(-z)$ and Eq. (A5) into the $H_m^{(2)}(z)$ expression, we have

$$H_m^{(2)}(z) = (-1)^m \left[H_m^{(2)}(-z) + 2J_m(-z)\right] \tag{A6}$$

Further, substituting Eqs. (A2) and (A3) into Eq, (A6), we finally reach

$$H_0^{(2)}(z) \sim \sqrt{\frac{-2}{\pi z}} \left[e^{j(z+\pi/4)} + 2\cos(z + \pi/4)\right] \tag{A7a}$$

$$H_1^{(2)}(z) \sim \sqrt{\frac{-2}{\pi z}} \left[-je^{j(z+\pi/4)} + 2\sin(z + \pi/4)\right] \tag{A7b}$$

From Eq. (A7), the second term of Eq. (1) is reduced to

$$\frac{1}{jv} \frac{H_1^{(2)}(-jv)}{H_0^{(2)}(-jv)} \approx \frac{1}{jv} \frac{3\tan(-jv + \pi/4) - j}{3 + j\tan(-jv + \pi/4)} \tag{A8}$$

APPENDIX B. THE DERIVATION FOR THE IMAGINARY PART OF U IN LOW FREQUENCY LIMIT TE CASE

As we discussed in Section 3.3 TE case, u has a large imaginary part. Therefore, substituting Eq. (29) into Eq. (19) with $\kappa = 1$ yields

$$\tanh u_I = u_I \Big/ \sqrt{r^2 + u_I^2} \tag{B1}$$

Further, Eq. (B1) is written as

$$(r^2 - u_I^2)(1 - e^{-2u_I}) = u_I^2(1 + e^{-2u_I})^2 \tag{B2}$$

After neglecting the higher order terms, we have

$$4u_I^2 e^{-2u_I} \approx r^2 \tag{B3}$$

which has a solution of $u_I = W_{-1}(-r/2)$. Similarly, substituting Eq. (29) into Eq. (25) with $\kappa = 1$ yields

$$\coth u_I \approx \frac{u_I}{\sqrt{r^2 + u_I^2}} \frac{3\coth u_I - 1}{3 - \coth u_I} \tag{B4}$$

Eq. (B4) will be reduced to Eq. (B3) with similar approximations. Consequently, the imaginary part of u is expressed as Eq. (30).

REFERENCES

1. Elsasser, W. M., "Attenuation in a dielectric circular rod," *J. Appl. Phys.*, Vol. 20, 1193–1196, 1949.
2. Jablonski, D., "Attenuation characteristics of circular dielectric waveguide at millimeter wavelengths," *IEEE Trans. Microw. Theory Techn.*, Vol. 26, No. 9, 667–671, 1978.
3. Jablonski, D., "Power-handling capabilities of circular dielectric waveguide at millimeter wave wavelengths," *IEEE Trans. Microw. Theory Techn.*, Vol. 33, No. 2, 85–89, 1985.
4. Kao, K. C., "Dielectric-fiber surface waveguide for optical frequencies," *Proc. IEE*, Vol. 133, No. 7, 1151–1158, 1966.
5. Snitzer, E., "Cylindrical dielectric waveguide modes," *J. Opt. Soc. Am.*, Vol. 51, No. 5, 491–498, 1961.
6. Safaai-Jazi, A. and G. L. Yip, "Classification of hybrid modes in cylindrical dielectric optical waveguides," *Radio Sci.*, Vol. 12, No. 4, 604–609, 1977.
7. Chatterjee, R., *Dielectric and Dielectric-Loaded Antennas*, John Wiley & Sons, Inc., 1985.
8. Zucker, F. J., H. Jasik,, Eds., *Antenna Engineering Handbook*, McGraw-Hill, New York, 1961.
9. Oliner, A. A., "Types and basic properties of leaky modes in microwave and millimeter wave integrated circuits," *IEICE Trans. Electron.*, Vol. 83, No. 5, 675–686, 2000.
10. Kobayashi, S., R. Mittra, and R. Lampe, "Dielectric tapered rod antennas for millimeter-wave applications," *IEEE Trans. Antennas Propag.*, Vol. 30, No. 1, 54–58, 1982.
11. Arnbak. J, "Leaky waves on a dielectric rod," *Electron. Lett.*, Vol. 1. 5, No. 3, 41–42, 1969.
12. Sammut, R., and A. W. Snyder, "Leaky modes on circular optical waveguides," *Appl. Opt.*, Vol. 15, No. 2, 477–482, 1976.
13. Kim, K. Y., "Guided and leaky modes of circular open electromagnetic waveguide," PhD thesis, Kyungpook National University, Daegu, Korea, 2004.
14. Kim, K. Y., H.-S. Tae, and J.-H. Lee, "Analysis of leaky modes in circular dielectric rod waveguides," *Electron. Lett.*, Vol. 39, No. 1, 61–62, 2003.
15. Lampariello, P., F. Frezza, H. Shigesawa, M. Tsuji, and A. A. Oliner, "A versatile leakywave antenna based on stub-loaded rectangular waveguide: Part I — Theory," *IEEE Trans. Microw. Theory Techn.*, Vol. 46, No. 7, 1032–1041, 1998.
16. Nallo, C. D., F. Frezza, A. Galli, P. Lampariello, and A. A. Oliner, "Properties of NRDguide and H-guide higher-order modes: Physical and Nonphysical ranges," *IEEE Trans. Microw. Theory Techn.*, Vol. 42, No. 12, 2429–2434, 1994.
17. Zeng, X. Y., S. J. Xu, K. Wu, and K. M. Luk, "Properties of guided modes on open structures near the cutoff region using a new version of complex effective dielectric constant," *IEEE Trans. Microw. Theory Techn.*, Vol. 50, No. 5, 1417–1424, 2002.

18. Lampariello, P., F. Frezza, and A. A. Oliner, "The transition region between bound-wave and leaky-wave ranges for a partially dielectric-loaded open guiding structure," *IEEE Trans. Microw. Theory Techn.*, Vol. 38, No. 12, 1831–1836, 1990.
19. Zhu, J. and Y. Lu, "Leaky modes of slab waveguides-asymptotic solutions," *J. Lightwave Techno.*, Vol. 24, No. 3, 1619–1623, 2006.
20. Rogier, H. and D. Vande Ginst, "A fast procedure to accurately determine leaky modes in multilayered planar dielectric substrates," *IEEE Trans. Microw. Theory Techn.*, Vol. 56, No. 6, 1413–1422, 2008.
21. Rogier, H. and D. De Zutter, "Berenger and leaky modes in optical fibers terminated with a perfectly matched layer," *J. Lightwave Techo.*, Vol. 20, No. 7, 1141–1148, 2002.
22. Vande Ginste, D., H. Rogier, and D. De Zutter, "Efficient computation of TM- and TE-polarized leaky modes in multilayered circular waveguides," *J. Lightwave Techo.*, Vol. 28, No. 11, 1661–1669, 2010.
23. Zhu, J., Z. Shen, and Z. Chen, "Dispersion relations of the modes for open nonhomogeneous waveguides terminated by perfectly matched layers," *J. Opt. Soc. Am. B*, Vol. 29, No. 9, 2524–2530, 2012.
24. *NIST Handbook of Mathematical Function*, Cambridge University Press, New York, 2010.
25. Corless, R., G. Gonnet, D. Hare, D. Jeffrey, and D. Knuth, "On the Lambert W function," *Adv. Comput. Math.*, Vol. 5, 329–359, 1996.
26. Zvorykin, V. D., A. O. Levchenko, A. V. Shutov, E. V. Solomina, N. N. Ustinovskii, and I. V. Smetanin, "Long-distance directed transfer of microwaves in tubular sliding-mode plasma waveguides produced by KrF laser in atmospheric air," *Phys. Plasmas*, Vol. 19, 033509, 2012.
27. Jin, J. M., *Theory and Computation of Electromagnetic Fields*, John Wiley & Sons, Inc., New York, 2010.
28. Balanis, C. A., *Advanced Engineering Electromagnetics*, John Wiley & Sons, Inc., New York, 1989.
29. Tsang, L. and B. P. Wu, "Electromagnetic fields of hertzian dipoles in layered media of moderate thickness including the effects of All modes," *IEEE Antennas Wireless Propag. Lett.*, Vol. 6, 316–319, 2007.
30. Shu, W. and J. M. Song, "Wave propagation in grounded dielectric slabs with double negative metamaterials," *Progress In Electromagnetics Research Symposium*, Vol. 2, No. 3, 246–250, 2006.
31. Kim, K. Y., "Comparative analysis of guided modal properties of double-positive and double-negative metamaterial slab waveguides," *Radioengineering*, Vol. 18, No. 2, 117–123, 2009.
32. Wang, Z. J. and J. F. Dong, "Analysis of guided modes in asymmetric left-handed slab waveguides," *Progress In Electromagnetics Research*, Vol. 62, 203–215, 2006.
33. Li, C., Q. Sui, and F. Li, "Complex guided wave solutions of grounded dielectric slab made of metamaterials," *Progress In Electromagnetics Research*, Vol. 51, 187–195, 2005.
34. Mahmoud, S. F. and A. J. Viitanen, "Surface wave character on a slab of metamaterial with negative permittivity and permeability," *Progress In Electromagnetics Research*, Vol. 51, 127–137, 2005.
35. Yang, S. M. and J. M. Song, "Guided and leaky modes of circular dielectric waveguide solved with multiple special functions," *IEEE Antennas and propagation Int. Symp.*, Paper 108.6, 125–126, 2014.
36. Yang, S. M. and J. M. Song, "Efficient initial guesses for solving guided and leaky modes in dielectric rod," *Annual Review of Progress in Applied Computational Electromagnetics*, 148–149, 2015.
37. Sommerfeld, A., *Electrodynamics*, translated by Ramberg, E. G., Academic Press, New York, 1952.
38. Ishimaru, A., *Electromagnetic Wave Propagation, Radiation, and Scattering*, Prentice Hall, Inc., 1991.
39. Chew, W. C., *Waves and Fields in Inhomogeneous Media*, IEEE Press, New York, 1995.